Published in final edited form as:
Dev Cell. 2007 September ; 13(3): 338–350. doi:10.1016/j.devcel.2007.07.017.

Failure of epithelial tube maintenance causes hydrocephalus and renal cysts in Dlg5$^{-/-}$ mice

Tamilla Nechiporuk[1], **Tania E. Fernandez**[1], and **Valeri Vasioukhin**[1,2,*]

1*Division of Human Biology, Fred Hutchinson Cancer Research Center, Seattle WA 98109, USA*

2*Department of Pathology and Institute for Stem Cell and Regenerative Medicine, University of Washington, Seattle, WA 98195, USA*

Abstract

Epithelial tubes represent fundamental building blocks of metazoan organisms; however, the mechanisms responsible for their formation and maintenance are not well understood. Here we show that unique and evolutionary conserved coiled-coil MAGUK protein, Dlg5, is required for epithelial tube maintenance in mammalian brain and kidneys. We demonstrate that *Dlg5*$^{-/-}$ mice develop fully penetrant hydrocephalus and kidney cysts caused by deficiency in membrane delivery of cadherin-catenin adhesion complexes and loss of cell polarity. Dlg5 travels with cadherin-containing vesicles and binds to syntaxin 4, a t-SNARE protein that regulates fusion of transport vesicles with the lateral membrane domain. We propose that Dlg5 functions in plasma membrane delivery of cadherins by linking cadherin-containing transport vesicles with the t-SNARE targeting complex. These findings identify a novel protein causally involved in hydrocephalus and renal cysts and reveal that targeted membrane delivery of cadherin-catenin adhesion complexes is critical for cell polarity and epithelial tube maintenance.

Introduction

Multicellular organisms contain a variety of epithelial and endothelial tubes that are used to channel the passage of liquids and gases. These tubes vary in size and shape, but they share central building principles. They are made by highly polarized cells with distinct basal, lateral and apical membrane domains. Defects in tube formation and maintenance are responsible for multiple human diseases, including obstructive hydrocephalus, kidney cysts, aneurysms and vaso-inclusive diseases. Despite the fundamental importance of tubes in human biology, the mechanisms responsible for tube formation and maintenance are only now beginning to be understood (Lubarsky and Krasnow, 2003).

Mammalian Dlg5/P-Dlg is a PDZ-containing (PSD-95, Dlg, ZO-1) MAGUK (membrane-associated guanylate kinase) protein with homology to Drosophila neoplastic tumor-suppressor discs large *dlg*. Sequence variation in human *DLG5* was initially reported to associate with inflammatory bowel disease; however, this association was not observed in some subsequent studies (Buning et al., 2006; Stoll et al., 2004). Based on sequence similarity, it has been

*Correspondence: Valeri Vasioukhin, Ph.D., Fred Hutchinson Cancer Research Center, 1100 Fairview Ave N C3-168, PO Box 19024, Seattle, WA 98109-1024, Phone: (206) 667-1710, Fax: (206) 667-6524, E-mail: vvasiouk@fhcrc.org

proposed that *Dlg5* is another vertebrate homolog of Drosophila *dlg*, hence the gene was named *Dlg5* (Nakamura et al., 1998). Here we show that *Dlg5* is distinct from the Dlg family and an evolutionary conserved gene with orthologs throughout the animal kingdom. We report that Dlg5 is necessary for the maintenance of epithelial tubes and *Dlg5*$^{-/-}$ mice develop fully penetrant obstructive hydrocephalus and renal cysts. We reveal that on the cellular level, brain and kidney abnormalities in *Dlg5*$^{-/-}$ mice result from the loss of cell polarity in the neural progenitor cells and epithelial cells lining the kidney collecting ducts. In addition, we report that on the molecular level Dlg5 is required for efficient delivery and stabilization of cadherin-catenin adhesion complex at the plasma membrane and interaction between Dlg5 and t-SNARE membrane targeting complex may be responsible for these functions.

Results

Dlg5 is distinct from the *Dlg* family and an evolutionary conserved gene

To determine the expression pattern of Dlg5, we performed Northern blot analyses (Figure 1A and data not shown). A single *Dlg5* transcript was expressed in multiple organs. The 7.8 kb size of Dlg5 mRNA was significantly larger than the originally published Dlg5 sequence (Nakamura et al., 1998). Analyses of mouse and human genome sequences revealed high similarity regions located upstream from *Dlg5*. We confirmed the presence of an additional coding exon in the Dlg5 sequence using RT-PCR and Northern blot experiments (data not shown). This exon of Dlg5 had an ATG surrounded by a strong Kozak consensus sequence and was coding for N-terminal CARD domain. Thus, the complete mouse Dlg5 cDNA encodes a large protein containing the CARD, Duff, Coiled-coil, four PDZs, SH3 and GUK domains (Figure 1B).

Blast analyses revealed orthologous *Dlg5* genes in evolutionary distant species, such as Drosophila *D. melanogaster* (GB#NM_135661), zebra fish *Danio rerio* (XP_697520.1) and chicken *Gallus gallus* (GB# XP_421604.1) (Figure 1B). The size and domain organization of Dlg5 differ from classic Dlg family proteins, which are devoid of the N-terminal CARD, Duff and Coiled-coil domains. Thus, we conclude that Dlg5 is a unique and evolutionary conserved protein. Evolutionary conservation of Dlg5 suggests a unique and important function.

Generation of *Dlg5* knockout mice

Dlg5 is an evolutionary conserved gene; however, its *in vivo* function is unknown, since no organisms with a mutation in *Dlg5* have been previously generated and characterized. To reveal the functional role of *Dlg5*, we generated *Dlg5* knockout mice (Figure 1C-F). The exon 2 was disrupted with IRES-β-geo-polyA cassette creating a stop codon after first 25 amino acids of Dlg5, lacking any functional domains. Western and Northern blot analyses showed complete absence of the Dlg5 protein and mRNA in these mice (Figure 1F and data not shown). We concluded that we generated mice with the null allele of *Dlg5*.

Closure of the aqueduct leads to severe hydrocephalus in *Dlg5*$^{-/-}$ brains

Although *Dlg5*$^{+/-}$ mice appeared indistinguishable from their wild-type counterparts, *Dlg5*$^{-/-}$ mice displayed growth retardation (Supplementary Figure 1). The mutant pups developed a characteristic dome-like appearance of their heads. Histological analyses of *Dlg5*$^{-/-}$ brains revealed fully penetrant hydrocephalus (n=20) with severe disorganization of the 3rd brain ventricle and massive dilation and fusion of the lateral brain ventricles (Figure 1G-G', Supplementary Figure 2). The surviving adult *Dlg5*$^{-/-}$ mice developed hopping gait (Supplementary video), similar to hydrocephalic *hyh* mice (Chae et al., 2004).

To determine the cellular defect responsible for hydrocephalus, we performed a histological survey of newborn *Dlg5*$^{-/-}$ brains. Aqueduct of Sylvius, a tube connecting the 3rd and 4th

ventricles of the brains, was closed in P0 *Dlg5*$^{-/-}$ brains (Figure 1H-I') (n=6). While the cells lining the aqueduct were well organized in the wild-type mice, they were disorganized and failed to keep the aqueduct open in *Dlg5*$^{-/-}$ brains (Figure 1I-J). We conclude that the closure of aqueduct is responsible for hydrocephalus in *Dlg5*$^{-/-}$ mice. Thus, Dlg5 is necessary for the maintenance of the epithelial tube and ventricular lining in the mammalian brain.

Hydrocephalus in *Dlg5*$^{-/-}$ brains is accompanied by loss of ependymal cells and disorganization of the subventricular stem cell niche

Ependymal cells form a continuous layer of multi-ciliated cells lining the ventricles (Spassky et al., 2005). Loss of ependymal cells, or denudation, can accompany hydrocephalus of various etiologies (Page, 1983; Sarnat, 1995). To study ependymal cells in *Dlg5*$^{-/-}$ brains, we analyzed the ventricular surface of P7 mice by histology and markers of ependymal cells (S100) and cilia (acetylated tubulin and polaris). While cuboidal multiciliated cells expressing S100, acetylated tubulin and polaris were present on the surface of the wild-type ventricles, these cells were absent in *Dlg5*$^{-/-}$ brains (Figure 1K-M'). Therefore, *Dlg5* is required for the formation of ependymal cells and ventricular surface is denuded in *Dlg5*$^{-/-}$ brains. Denudation of the ventricular lining may disturb normal flow of CSF and contribute to hydrocephalus in *Dlg5*$^{-/-}$ brains.

Histological analyses of lateral ventricles from P7-P21 *Dlg5*$^{-/-}$ brains revealed foci of abnormal cell accumulation, randomly distributed along the ventricular surface (Supplementary Figure 3A-C'). These foci contained a heterogeneous population of proliferating cells expressing glial fibrillary acidic protein, GFAP (stem cells and astrocytes marker (Garcia et al., 2004)), Dcx2 (transient-amplifying cells marker (Doetsch et al., 2002)) and nestin (neural progenitor cells marker (Lendahl et al., 1990)) and did not express ependymal cell marker S100 (Supplementary Figure 3D-J'). The cell-type specific staining pattern and histology of dysplastic foci of *Dlg5*$^{-/-}$ brains was remarkably similar to the stem cell niche in the subventricular zone in wild-type brains. We conclude that in the absence of ependymal cell layer in *Dlg5*$^{-/-}$ brains, cells in the subventricular zone become disorganized and form dysplastic foci.

Disruption of epithelial cell polarity, loss of cilia and kidney cysts in *Dlg5*$^{-/-}$ mice

In addition to tube maintenance defects in brain, *Dlg5*$^{-/-}$ mice also displayed severe epithelial tube maintenance defects in kidneys. Histological examination of *Dlg5*$^{-/-}$ kidneys revealed the formation of renal cysts (Figure 2A-A'). The phenotype was fully penetrant and varied from small cysts-like structures to large fluid-filled cysts. The large cysts were not lined by the polarized epithelial layer, but instead displayed a fibrous surface (inset in Figure 2A'). The blood urea nitrogen (BUN) levels were significantly higher in the mutant mice suggesting impaired kidney function (Figure 2B). Whereas newborn *Dlg5*$^{-/-}$ kidneys were histologically undistinguishable from wild-type counterparts, we observed dilations in kidney collecting ducts in the pelvis of P3 *Dlg5*$^{-/-}$ kidneys (Figure 2E-E'). Immunostainings with cell-type-specific markers revealed that the majority of cysts in *Dlg5*$^{-/-}$ kidneys were of the collecting duct origin (Figure 2C-D). Interestingly, we found that collecting ducts express high levels of Dlg5 in the wild-type mice (Supplementary Figure 4).

Epithelial cells in the collecting ducts are highly polarized and contain distinct apical, lateral and basal membrane domains. Immunofluorescence stainings of collecting ducts for the cell polarity marker aPKC revealed that while all wild-type tubes displayed apical localization of aPKC, many tubes in *Dlg5*$^{-/-}$ kidneys show loss of apical localization of aPKC, suggesting early defects in cell polarity (Figure 2G-G'). In addition, dilated collecting ducts in *Dlg5*$^{-/-}$ kidneys failed to express the apical membrane marker Aquaporin-2 (Figure 2F, J and Supplementary Figure 5). Immunostaining for the lateral membrane marker, E-cadherin, revealed the presence of distinct lateral membrane domain in *Dlg5*$^{-/-}$ cells; however, E-cadherin

staining was disorganized and appeared more diffuse in mutant cells (Figure 2G-G'). Formation of renal cysts may result from abnormalities in primary cilia, representing extensions of the apical membrane domain (Zhang et al., 2004). Immunostaining with anti-acetylated-tubulin antibodies (cilia marker) revealed that, while cilia were present on *Dlg5*$^{-/-}$ cells lining nondilated tubes, they were missing on cells lining dilated tubes and cysts-like structures (Figure 2H-I). We concluded that loss of cell polarity and the subsequent loss of cilia are the earliest detectable defects that coincide with or precede the formation of epithelial cysts in *Dlg5*$^{-/-}$ mice.

To reveal additional defects in kidneys of *Dlg5*$^{-/-}$ mice, we performed cross sections through the kidney pelvic region, uretero-pelvic junction (UPJ) and ureter. In contrast to well-organized and open kidney pelvis papillary ducts at the UPJs in wild-type mice, papillary ducts in *Dlg5*$^{-/-}$ kidneys were disorganized and often failed to maintain tube openings (Figure 2K-K', 2 out of 6 mice). In addition, *Dlg5*$^{-/-}$ ureter displayed constriction (4 out of 6 mice) and formation of ureteral polyps (2 out of 6 mice) (Figure 2L-L‴). These abnormalities may result in partial obstruction of the flow of urine in *Dlg5*$^{-/-}$ kidneys and contribute to renal cyst formation in *Dlg5*$^{-/-}$ mice. Therefore, in addition to classic polycystic kidney defects, *Dlg5*$^{-/-}$ kidneys showed occasional occlusion of collecting ducts, constriction of the ureter and formation of ureteral polyps (Figure 2K-L‴). These abnormalities are characteristic to congenital obstructive hydronephrosis. Combination of abnormalities characteristic to both polycystic kidney disease and hydronephrosis may be a unique hallmark of *Dlg5*$^{-/-}$ kidneys.

Loss of cell polarity and disorganization of apical junctional adhesion complexes in *Dlg5*$^{-/-}$ neural progenitors

Similar to kidney collecting ducts, brain ventricular surfaces are also lined with highly polarized cells, which are organized as pseudostratified epithelium containing cilia at the apical membrane domain and forming prominent apical-junctional adhesion complexes at the ventricular surface (Chenn et al., 1998). To determine whether loss of cell polarity in *Dlg5*$^{-/-}$ neural progenitors may be responsible for closure of the aqueduct, we analyzed this area of the brain early in development. While *Dlg5*$^{-/-}$ progenitors from E13.5 brains were undistinguishable from their wild-type counterparts, progenitors in E15.5 mice were disorganized and failed to form a polarized epithelial layer (Figure 3A-B'). Stainings with cell polarity markers pericentrin (centrosomal and cilia basal body marker) and aPKC (apical membrane marker) revealed loss of polarity in *Dlg5*$^{-/-}$ progenitor cells (Figure 3C-D'). In addition, while apical junctional complex proteins N-cadherin, β-catenin and ZO-1 were localized at the ventricular surface of the wild-type progenitors, these proteins were mislocalized in *Dlg5*$^{-/-}$ cells (Figure 3E-G'). Instead of accumulation at the ventricular surface, the adherens junction (AJ) protein N-cadherin displayed punctate cytoplasmic localization in *Dlg5*$^{-/-}$ progenitors (Figure 3E'). Defects in epithelial layer maintenance, polarity and adhesion in embryonic *Dlg5*$^{-/-}$ progenitors were found primarily around the 3rd ventricle and future aqueduct region, and they were not as prominent in other regions of the brain. This selectivity can be at least partially explained by the prominent expression of Dlg5 in areas of the 3rd ventricle and aqueduct in the wild-type mice (Supplementary Figure 4).

Defects in localization of AJ proteins in *Dlg5*$^{-/-}$ cells were potentially interesting because disruption of AJs in embryonic brain can lead to loss of polarity and disorganization of neural progenitors (Lien et al., 2006). We found that Dlg5 co-localized with β-catenin in neural progenitor cells *in vivo* (Figure 3H-H'). In addition, GFP-tagged E-cadherin and Strawberry-tagged Dlg5 co-localize at the AJs in stably transfected mammalian MDCK cells (Supplementary Figure 6). Therefore, we hypothesized that Dlg5 was necessary for proper localization of AJ proteins, and loss of Dlg5 could have resulted in disorganization of AJs and

a subsequent loss of polarity, cell adhesion, and ultimately, failure of epithelial tube maintenance.

Impaired cadherin-catenin complex formation and decreased cell-surface levels of N-cadherin in *Dlg5*$^{-/-}$ progenitor cells

Since immunostaining revealed mislocalization of AJ proteins in *Dlg5*$^{-/-}$ brains, we used a biochemical approach to analyze the subcellular distribution of N-cadherin and β-catenin in more detail. To determine whether N-cadherin is properly localized at the cell surface in *Dlg5*$^{-/-}$ cells, we analyzed the cell surface levels of N-cadherin in *Dlg5*$^{-/-}$ progenitors. We found that despite overall similar levels of N-cadherin between wild-type and mutant cells, cell surface levels of N-cadherin and β-catenin, associated with N-cadherin, were significantly reduced in *Dlg5*$^{-/-}$ progenitors (Figure 4A-A'). We conclude that Dlg5 is necessary for cell surface stabilization of cadherin-catenin protein complex in neural progenitor cells. Remarkably, these changes were not restricted to progenitors around the 3rd ventricle, but were seen in total brain neural progenitors, suggesting proper localization of cadherin-catenin complex is a general function of Dlg5.

We next analyzed whether Dlg5 is necessary for the integrity of AJ. Co-immunoprecipitation experiments revealed decreased levels of N-cadherin and α-catenin in the cadherin-catenin complexes immunoprecipitated from *Dlg5*$^{-/-}$ brains with anti-β-catenin antibodies (Figure 4B-B'). In addition, co-immunoprecipitation experiments indicate that Dlg5 physically interacts with β-catenin in the wild-type brain (Figure 4B). We found two β-catenin-binding sites in Dlg5: in its N-terminal and PDZ3-4 domains (Figure 4C-E). Dlg5 was interacting not only with β-catenin, but also with cadherin, revealing the existence of cadherin-β-catenin-Dlg5 protein complexes (Supplementary Figure 7).

Coiled-coil domain of Dlg5 is a unique feature that distinguishes it from all other Dlg family members. Self-association is one of potential functions of coiled-coil domains. To determine whether Dlg5 can self-associate, we performed co-immunoprecipitation experiments with a variety of tagged Dlg5 proteins. Dlg5 displayed prominent self-association and subsequent experiments revealed that the N-terminal part containing coiled-coil domain was primarily responsible for this function (Figure 5). In addition, PDZ3-PDZ4 and SH3-GUK domains of Dlg5 also displayed self-association abilities and were able to bind to the N-terminal part of Dlg5, indicating an additional possibility of a head to tail oligomerization or intramolecular interaction of the N-terminus with the C-terminus of the protein. Self-association of Dlg5 could result in formation of large protein complexes containing multiple β-catenin-binding domains that can scaffold and stabilize cadherin-catenin complexes at the plasma membrane.

Impaired cell surface delivery and stabilization of N-cadherin-catenin complex in *Dlg5*$^{-/-}$ MEF cells

To investigate the mechanism of Dlg5 function responsible for localization of cadherin-catenin complexes to the AJ, we utilized primary mouse embryonic fibroblasts (MEFs). Similar to neural progenitor cells, MEFs depend on N-cadherin to form AJs (Teng et al., 2005). We found that *Dlg5*$^{-/-}$ MEFs also exhibited significantly reduced levels of cell-surface N-cadherin (Figure 6A-A'), and displayed decreased junctional localization of AJ proteins N-cadherin, β-catenin and p120-catenin (Supplementary Figure 8). Reduced levels of cell-surface N-cadherin can result from deficient delivery or stabilization of the protein at the plasma membrane. To determine which of these functions was impaired in *Dlg5*$^{-/-}$ MEFs, we performed pulse chase experiments to follow-up cell surface appearance and retention of ^{35}S-labeled N-cadherin (Davis et al., 2003; Teng et al., 2005). The levels and dynamics of cell-surface appearance of N-cadherin in *Dlg5*$^{-/-}$ MEFs revealed defects in both delivery and stabilization of the protein

at the plasma membrane (Figure 6B-B', n=4). We conclude that Dlg5 is necessary for cell-surface delivery and stabilization of cadherin-catenin complexes.

Dlg5 localizes to AJs and N-cadherin-containing vesicles and facilitates delivery of N-cadherin to the AJs in live MEFs

In normal cells newly-synthesized N-cadherin quickly associates with β-catenin and is delivered from the Golgi to the plasma membrane via secretory vesicles (Mary et al., 2002). To analyze the dynamics of Dlg5 and N-cadherin in live cells, we electroporated wild-type and *Dlg5*$^{-/-}$ MEFs with N-cadherin-GFP and Strawberry-Dlg5 expression constructs. We found that 20 hrs post-electroporation, N-cadherin-GFP was localizing to the cytoplasmic vesicles and the AJs in wild-type MEFs (Figure 6C-E", green). Interestingly, Strawberry-Dlg5 also showed vesicular, and to a lower degree, AJs localization that significantly, but not completely, overlapped with N-cadherin-GFP (Figure 6C-E", red). Remarkably, while the majority of the wild-type cells electroporated with N-cadherin-GFP (89%) displayed the protein at the AJs at 20 hrs after transfection, only half (49%) of the *Dlg5*$^{-/-}$ MEFs showed junctional N-cadherin-GFP (Figure 6G-H). The majority of N-cadherin-GFP in mutant cells was localized to the cytoplasmic perinuclear vesicles. Simultaneous electroporation of *Dlg5*$^{-/-}$ MEFs with N-cadherin-GFP and Strawberry-Dlg5 constructs partially rescued this defect (Figure 6F,G", H). To determine the identity of Dlg5-positive vesicles, we stained MEFs and MDCK cells with a series of vesicle markers including Rab-11, marker of recycling endosomes, Rab-8, marker of trans-Golgi vesicles, Rab-5 and EEA1, early endosomal markers, and GM130, Golgi marker. While Dlg5-containing vesicles were negative for Rab-5, Rab-8, EEA1, and GM130 (data not shown), we found partial overlap between Rab-11 and Dlg5-positive vesicles (Supplementary Figure 9). Interestingly, cadherin-carrying transport vesicles fuse with Rab-11-positive endosomes on their route to the plasma membrane (Lock and Stow, 2005). We conclude that Dlg5 accompanies newly synthesized N-cadherin as it is transported from the Golgi to the plasma membrane.

Dlg5 binds to syntaxin 4 and may facilitate targeted cadherin delivery by linking cadherin-catenin-carrying transport vesicles with the t-SNARE complex at the plasma membrane

Efficient and targeted delivery of N-cadherin requires tethering and a SNARE-dependent fusion of N-cadherin-β-catenin-containing vesicles with the AJs. We hypothesized that Dlg5 may facilitate targeted membrane delivery of cadherin-catenin complex by interacting with the SNARE membrane fusion machinery. We analyzed potential interactions between Dlg5 and SNARE proteins and found that endogenous Dlg5 in brains and kidneys physically associates with syntaxin 4 (Figure 7A-B), a t-SNARE protein responsible for vesicle delivery to the basolateral membrane domain (ter Beest et al., 2005). This interaction was specific for syntaxin 4, as we found no binding between Dlg5 and syntaxins 2 and 3 (data not shown). Syntaxin 4 co-localized with Dlg5 on cytoplasmic vesicles and AJs (Figure 7 D-E‴). Co-transfection experiments with full-length and truncated fragments of Dlg5 revealed that PDZ1-2 and PDZ3-4 domains of Dlg5 are involved in interaction with syntaxin 4 (Figure 7C and Supplementary Figure 10). It is likely that these domains have a redundant function, because deletion of either PDZ1-2 or PDZ3-4 domains was not sufficient for generation of the nonfunctional protein (Supplementary Figure 11).

To summarize, we propose that Dlg5 utilizes its multiple β-catenin and syntaxin 4-binding domains to link cadherin-carrying transport vesicles to the t-SNARE vesicle targeting complex at the lateral membrane domain of polarized cells (Figure 7F). In addition, it can potentially use its self-association and β-catenin-binding regions to cluster and stabilize cadherin-catenin complexes at the AJs. These mechanisms can ensure targeted delivery and stabilization of cadherin-catenin complexes to maintain polarity of cells forming epithelial tubes.

Discussion

Maintenance of cell polarity by targeted plasma membrane delivery and stabilization of cadherin-catenin complex is a critical function of Dlg5

Dlg5 is a member of MAGUK family proteins. These molecules, especially the Dlgs, have been implicated in regulation of membrane protein targeting. Mammalian Dlg1/SAP97 and Dlg4/PSD-95 are involved in synaptic membrane clustering of AMPA receptors and ion channel proteins (Cai et al., 2006; Tiffany et al., 2000). While *Dlg2/PSD-93*$^{-/-}$ mice do not show avert abnormalities, *Dlg4/PSD-95*$^{-/-}$ mice live and are fertile, but show learning disabilities due to changes in synaptic transmission (McGee et al., 2001; Migaud et al., 1998). Mice with truncation of *Dlg1* display craniofacial malformations (Caruana and Bernstein, 2001), and *Dlg1*$^{-/-}$ animals show misorientation of smooth muscle cells in the ureter (Mahoney et al., 2006). Dlg5 is a unique MAGUK protein. While it shares many structural features with Dlg family proteins, it contains a unique N-terminus carrying the coiled-coil, Duff and CARD domains. Similar to other Dlgs, Dlg5 facilitates membrane protein targeting. However, instead of targeting and clustering the synaptic proteins, Dlg5 function is more general, as it is necessary for targeting and retention of the cadherin-catenin adhesion complex in many different cell types. Since mechanisms responsible for function of classic mammalian Dlgs (PSD-95, PSD-93, SAP-102) in synaptic targeting are still poorly understood, it will be interesting to determine whether described here interaction between Dlg5 and the t-SNARE transport vesicle fusion machinery represents a function conserved in other Dlg proteins.

Disorganization of intercellular adhesion and loss of cell polarity as a causal factor in obstructive hydrocephalus and renal cysts in *Dlg5*$^{-/-}$ mice

Loss of cell polarity and tissue disorganization is the primary cellular defect responsible for hydrocephalus in *Dlg5*$^{-/-}$ animals. Indeed, non-polarized and disorganized progenitors in developing *Dlg5*$^{-/-}$ brain are unable to maintain proper tube architecture and fail to keep the aqueduct open. This results in obstruction of the ventricular liquid flow and subsequent hydrocephalus. Similar to Dlg5 mutants, disruption of intercellular adhesion and disorganization of neural progenitors is responsible for closure of the aqueduct and severe hydrocephalus in *myosin IIB*$^{-/-}$ mice (Tullio et al., 2001). In addition, humans and mice with mutations in cell adhesion molecule L1, display closure of the aqueduct and hydrocephalus (Itoh et al., 2004). Mutation in αSNAP protein, a receptor for SNARE complex involved in polarized membrane targeting, causes disruption in localization of apical-junctional proteins and results in obstructive hydrocephalus (Chae et al., 2004). Overall, despite complex genetic causes of obstructive hydrocephalus, the abnormalities involving the disruption of adhesion and cell polarity of neural progenitor cells may represent a common cellular defect responsible for this devastating disease.

Similarly to the developing brain, cell polarity is critical for proper morphogenesis and maintenance of epithelial tubes in mammalian kidney. We found that *Dlg5*$^{-/-}$ kidney develop dilation of collecting ducts and formation of cysts. Majority of proteins implicated in mammalian polycystic kidney disease localize to the epithelial junctions and primary cilium and some of these proteins are also involved in hydrocephalus (Harris and Torres, 2006; Taulman et al., 2001). Primary cilium is an apical membrane extension and cilia retention is likely to require proper maintenance of epithelial cell polarity. *Dlg5*$^{-/-}$ animals develop early defects in polarized localization of aPKC, which are followed by the loss of cilia. It is likely that disruption of cell polarity in *Dlg5*$^{-/-}$ cells affects cilia maintenance, which results in subsequent epithelial cysts formation.

In summary, we report a novel gene responsible for mammalian hydrocephalus and renal cysts. We report that Dlg5 is required for maintenance of AJs and epithelial cell polarity in

mammalian brain and kidneys. At the molecular level, Dlg5 is necessary for cell-surface delivery and stabilization of cadherin-catenin adhesion complexes. Finally, we demonstrate that Dlg5 binds to t-SNARE basolateral vesicle targeting machinery and also travels with cadherin-catenin-carrying transport vesicles. We propose that Dlg5 uses its unique N-terminal self-association domain to tether cadherin-containing transport vesicles to the t-SNARE complex to ensure polarized membrane delivery of AJs proteins.

Experimental Procedures

Generation of *Dlg5*$^{-/-}$ mice

Dlg5-null allele in ES cells was generated using standard DNA recombination technology (Hogan, 1994). Generated from ES cells chimeras were crossed to C57/BL6 mice and the resulting heterozygous animals were crossed with each other to produce the *Dlg5*$^{-/-}$ mice. Mouse genotyping was performed by PCR with oligos: PGKFwd2: 5′-ATTGCATCGCATTGTCTGAGTAGGTG-3′, Dlg5B11: 5′-CATGGTGCAATGCAACTTCCTC-3′; and Dlg5 A14: 5′-TGCTACTGCTGCAGAGTCCTCC-3′. The wild-type allele of Dlg5 is amplified by B11-A14 primer pair and the knockout allele is amplified by the PGKFwd2-Dlg5B11 pair.

Immunofluorescence, Western blot analyses, immunoprecipitation, and antibodies

Immunofluorescent staining, immunoprecipitation and Western blot analysis were performed as described (Klezovitch et al., 2004). Fixed and stained, or live cells were analyzed using a Zeiss fluorescent microscope in 0.2 micron Z-steps and deconvoluted using Deltavision. Antibodies used: anti-β-tubulin III, anti-β-actin, anti-GFAP, anti-S100 (Sigma), anti-nestin (Developmental Studies Hybridoma Bank), anti-Ki67 (Novocastra), anti-N-cadherin, anti-ZO1 (Zymed), anti-Rab11, anti-Rab5, anti-Rab8, anti-GM130 (BD Biosciences), anti-EEA1 (AffinityBioreagents), anti-aPKC (Santa Cruz), anti-aquaporin-2 (gift from M. Knepper), *Dolichos Biflorius* agglutinin (Vector laboratories), anti-Tamm Horstall protein (Biomedical Technologies), anti-Dcx2 (Chemicon), anti-syntaxin 4 (SYSY), anti-V5(Invitrogen). Anti-Dlg5 antibodies were generated in rabbits using GST-Dlg5 fusion containing 204 amino acids (aa) of mouse Dlg5 (aa1139-1343, GB#147699) (Proteintech Group). Antibodies were affinity purified using sequential GST-sepharose depletion and GST-Dlg5 affinity purification.

DNA constructs

The coding sequence of Dlg5, syntaxin4 and Dlg5 deletion constructs were generated by PCR, subcloned into pENTRY vector, and subsequently transferred into pDestV5 or pDest53 vectors (Invitrogen). Full-length N-cadherin was cloned into pEGFP-N1 vector to generate C-terminal GFP fusion. Strawberry sequence from pRSET plasmid was PCR amplified and N-terminally fused to full-length Dlg5 in pCMVSport6 vector. All expression constructs were verified by sequencing.

Cell culture and biochemical studies

Primary MEFs were isolated and maintained as described (Hogan, 1994). MEFs and HEK 293 cells were maintained in DMEM media supplemented with 10% Fetal Bovine serum, glutamine, non-essential amino acids and antibiotics. MEFs were electroporated using MEF1 reagent (Amaxa). HEK 293 cells were transfected using calcium phosphate precipitation. MDCK cells stably expressing E-cadherin-EGFP were co-transfected with Strawberry-Dlg5 and pBabe (puro) vector and were clonally selected for puromycin resistance and red fluorescent Dlg5.

Steady-state and pulse-chase kinetics of N-cadherin

Primary neural progenitor cells were isolated by trypsin digestion in the presence of Ca^{2+}/Mg^{2+} to preserve transmembrane cadherins (Bonifacino, 1998; Johansson et al., 1999). Cell surface proteins were labeled with cell-impermeable biotin (Pierce), followed by inactivation of biotin label and lysis of the cells. Biotinylated surface proteins were pulled down with streptavidin beads and analyzed by Western blotting. Steady-state cell surface and total levels of N-cadherin were determined by Western blotting with anti-N-cadherin antibodies (Teng et al., 2005). For pulse-chase analysis of cell surface delivery of N-cadherin MEFs were labeled with ^{35}S methionine/cysteine for 20 min, washed and chased for various times prior to surface biotinylation and lysis. To obtain total and cell surface level of N-cadherin, sequential IP with anti-N-cadherin antibodies followed by pulldown on streptavidin sepharose was used as described (Davis et al., 2003). Quantitation of junctional levels of AJ proteins in MEFs was performed as described (Teng et al., 2005).

In situ hybridization

In situ hybridization on cryosections was performed as described (Sciavolino et al., 1997). 919 bp *Dlg5* cDNA fragment, was amplified with primers 5′ GTTCTGCAGATGCCCACTTGAGG 3′ and 5′ CGCATGAGATTCCAGAATTGTCC 3′, subcloned into a PCR-4-TOPO vector (Invitrogen), linearized and transcribed to obtain sense and antisense RNA probes (Ambion).

BUN analyses

Blood was collected from mice orbital sinus and processed by Phoenix Central Laboratory (Everett, WA).

Supplementary Material

Refer to Web version on PubMed Central for supplementary material.

Acknowledgements

We thank P. Soriano, S. Parkhurst, J. Cooper, B. Helbing and all members of Vasioukhin laboratory for critical reading of this manuscript; J.W. Nelson for the gift of E-cadherin-GFP expressing MDCK cells; R.Y. Tsien for the gift of mStrawberry; M. Knepper and Developmental Studies Hybridoma Bank for the gift of antibodies; Marino Zerial for Rab-11-GFP construct; Nanyan Jiang for injections of ES cells; Olga Klezovitch for maintenance of *Dlg5*$^{-/-}$ mice and timed pregnancies; Linda Cherepow for help with histology. This work was supported by R01 CA098161, R01 CA102365 (to VV) and Chromosome Metabolism and Cancer Training Grant NIH T32 CA09657, Viral Oncology Training Grant NIH T32 CA09229 (to TN).

REFERENCES

Bonifacino, JS. Current protocols in cell biology. John Wiley; New York: 1998.

Buning C, Geerdts L, Fiedler T, Gentz E, Pitre G, Reuter W, Luck W, Buhner S, Molnar T, Nagy F, et al. DLG5 variants in inflammatory bowel disease. Am J Gastroenterol 2006;101:786–792. [PubMed: 16494592]

Cai C, Li H, Rivera C, Keinanen K. Interaction between SAP97 and PSD-95, two Maguk proteins involved in synaptic trafficking of AMPA receptors. J Biol Chem 2006;281:4267–4273. [PubMed: 16332687]

Caruana G, Bernstein A. Craniofacial dysmorphogenesis including cleft palate in mice with an insertional mutation in the discs large gene. Mol Cell Biol 2001;21:1475–1483. [PubMed: 11238884]

Chae TH, Kim S, Marz KE, Hanson PI, Walsh CA. The hyh mutation uncovers roles for alpha Snap in apical protein localization and control of neural cell fate. Nat Genet 2004;36:264–270. [PubMed: 14758363]

Chenn A, Zhang YA, Chang BT, McConnell SK. Intrinsic polarity of mammalian neuroepithelial cells. Mol Cell Neurosci 1998;11:183–193. [PubMed: 9675050]

Davis MA, Ireton RC, Reynolds AB. A core function for p120-catenin in cadherin turnover. J Cell Biol 2003;163:525–534. [PubMed: 14610055]

Doetsch F, Petreanu L, Caille I, Garcia-Verdugo JM, Alvarez-Buylla A. EGF converts transit-amplifying neurogenic precursors in the adult brain into multipotent stem cells. Neuron 2002;36:1021–1034. [PubMed: 12495619]

Francis F, Koulakoff A, Boucher D, Chafey P, Schaar B, Vinet MC, Friocourt G, McDonnell N, Reiner O, Kahn A, et al. Doublecortin is a developmentally regulated, microtubule-associated protein expressed in migrating and differentiating neurons. Neuron 1999;23:247–256. [PubMed: 10399932]

Garcia AD, Doan NB, Imura T, Bush TG, Sofroniew MV. GFAP-expressing progenitors are the principal source of constitutive neurogenesis in adult mouse forebrain. Nat Neurosci 2004;7:1233–1241. [PubMed: 15494728]

Harris PC, Torres VE. Understanding pathogenic mechanisms in polycystic kidney disease provides clues for therapy. Curr Opin Nephrol Hypertens 2006;15:456–463. [PubMed: 16775462]

Hogan, B. Manipulating the mouse embryo: a laboratory manual. Vol. 2nd edn. Cold Spring Harbor Laboratory Press; Plainview, N.Y.: 1994.

Itoh K, Cheng L, Kamei Y, Fushiki S, Kamiguchi H, Gutwein P, Stoeck A, Arnold B, Altevogt P, Lemmon V. Brain development in mice lacking L1-L1 homophilic adhesion. J Cell Biol 2004;165:145–154. [PubMed: 15067019]

Johansson CB, Momma S, Clarke DL, Risling M, Lendahl U, Frisen J. Identification of a neural stem cell in the adult mammalian central nervous system. Cell 1999;96:25–34. [PubMed: 9989494]

Klezovitch O, Fernandez TE, Tapscott SJ, Vasioukhin V. Loss of cell polarity causes severe brain dysplasia in Lgl1 knockout mice. Genes Dev 2004;18:559–571. [PubMed: 15037549]

Lendahl U, Zimmerman LB, McKay RD. CNS stem cells express a new class of intermediate filament protein. Cell 1990;60:585–595. [PubMed: 1689217]

Lien WH, Klezovitch O, Fernandez TE, Delrow J, Vasioukhin V. alphaE-catenin controls cerebral cortical size by regulating the hedgehog signaling pathway. Science 2006;311:1609–1612. [PubMed: 16543460]

Lock JG, Stow JL. Rab11 in recycling endosomes regulates the sorting and basolateral transport of E-cadherin. Mol Biol Cell 2005;16:1744–1755. [PubMed: 15689490]

Lubarsky B, Krasnow MA. Tube morphogenesis: making and shaping biological tubes. Cell 2003;112:19–28. [PubMed: 12526790]

Mahoney ZX, Sammut B, Xavier RJ, Cunningham J, Go G, Brim KL, Stappenbeck TS, Miner JH, Swat W. Discs-large homolog 1 regulates smooth muscle orientation in the mouse ureter. Proc Natl Acad Sci U S A 2006;103:19872–19877. [PubMed: 17172448]

Mary S, Charrasse S, Meriane M, Comunale F, Travo P, Blangy A, Gauthier-Rouviere C. Biogenesis of N-cadherin-dependent cell-cell contacts in living fibroblasts is a microtubule-dependent kinesin-driven mechanism. Mol Biol Cell 2002;13:285–301. [PubMed: 11809840]

McGee AW, Topinka JR, Hashimoto K, Petralia RS, Kakizawa S, Kauer FW, Aguilera-Moreno A, Wenthold RJ, Kano M, Bredt DS. PSD-93 knock-out mice reveal that neuronal MAGUKs are not required for development or function of parallel fiber synapses in cerebellum. J Neurosci 2001;21:3085–3091. [PubMed: 11312293]

Migaud M, Charlesworth P, Dempster M, Webster LC, Watabe AM, Makhinson M, He Y, Ramsay MF, Morris RG, Morrison JH, et al. Enhanced long-term potentiation and impaired learning in mice with mutant postsynaptic density-95 protein. Nature 1998;396:433–439. [PubMed: 9853749]

Nakamura H, Sudo T, Tsuiki H, Miyake H, Morisaki T, Sasaki J, Masuko N, Kochi M, Ushio Y, Saya H. Identification of a novel human homolog of the Drosophila dlg, P-dlg, specifically expressed in the gland tissues and interacting with p55. FEBS Lett 1998;433:63–67. [PubMed: 9738934]

Page, R.; Leuredu-Pree, AE. Ependymal alterations in hydrocephalus. Vol. 2. Plenum Press; New York: 1983.

Sarnat HB. Ependymal reactions to injury. A review. J Neuropathol Exp Neurol 1995;54:1–15. [PubMed: 7815072]

Sciavolino PJ, Abrams EW, Yang L, Austenberg LP, Shen MM, Abate-Shen C. Tissue-specific expression of murine Nkx3.1 in the male urogenital system. Dev Dyn 1997;209:127–138. [PubMed: 9142502]

Spassky N, Merkle FT, Flames N, Tramontin AD, Garcia-Verdugo JM, Alvarez-Buylla A. Adult ependymal cells are postmitotic and are derived from radial glial cells during embryogenesis. J Neurosci 2005;25:10–18. [PubMed: 15634762]

Stoll M, Corneliussen B, Costello CM, Waetzig GH, Mellgard B, Koch WA, Rosenstiel P, Albrecht M, Croucher PJ, Seegert D, et al. Genetic variation in DLG5 is associated with inflammatory bowel disease. Nat Genet 2004;36:476–480. [PubMed: 15107852]

Taulman PD, Haycraft CJ, Balkovetz DF, Yoder BK. Polaris, a protein involved in left-right axis patterning, localizes to basal bodies and cilia. Mol Biol Cell 2001;12:589–599. [PubMed: 11251073]

Teng J, Rai T, Tanaka Y, Takei Y, Nakata T, Hirasawa M, Kulkarni AB, Hirokawa N. The KIF3 motor transports N-cadherin and organizes the developing neuroepithelium. Nat Cell Biol 2005;7:474–482. [PubMed: 15834408]

ter Beest MB, Chapin SJ, Avrahami D, Mostov KE. The role of syntaxins in the specificity of vesicle targeting in polarized epithelial cells. Mol Biol Cell 2005;16:5784–5792. [PubMed: 16207812]

Tiffany AM, Manganas LN, Kim E, Hsueh YP, Sheng M, Trimmer JS. PSD-95 and SAP97 exhibit distinct mechanisms for regulating K(+) channel surface expression and clustering. J Cell Biol 2000;148:147–158. [PubMed: 10629225]

Tullio AN, Bridgman PC, Tresser NJ, Chan CC, Conti MA, Adelstein RS, Hara Y. Structural abnormalities develop in the brain after ablation of the gene encoding nonmuscle myosin II-B heavy chain. J Comp Neurol 2001;433:62–74. [PubMed: 11283949]

Zhang Q, Taulman PD, Yoder BK. Cystic kidney diseases: all roads lead to the cilium. Physiology (Bethesda) 2004;19:225–230. [PubMed: 15304637]

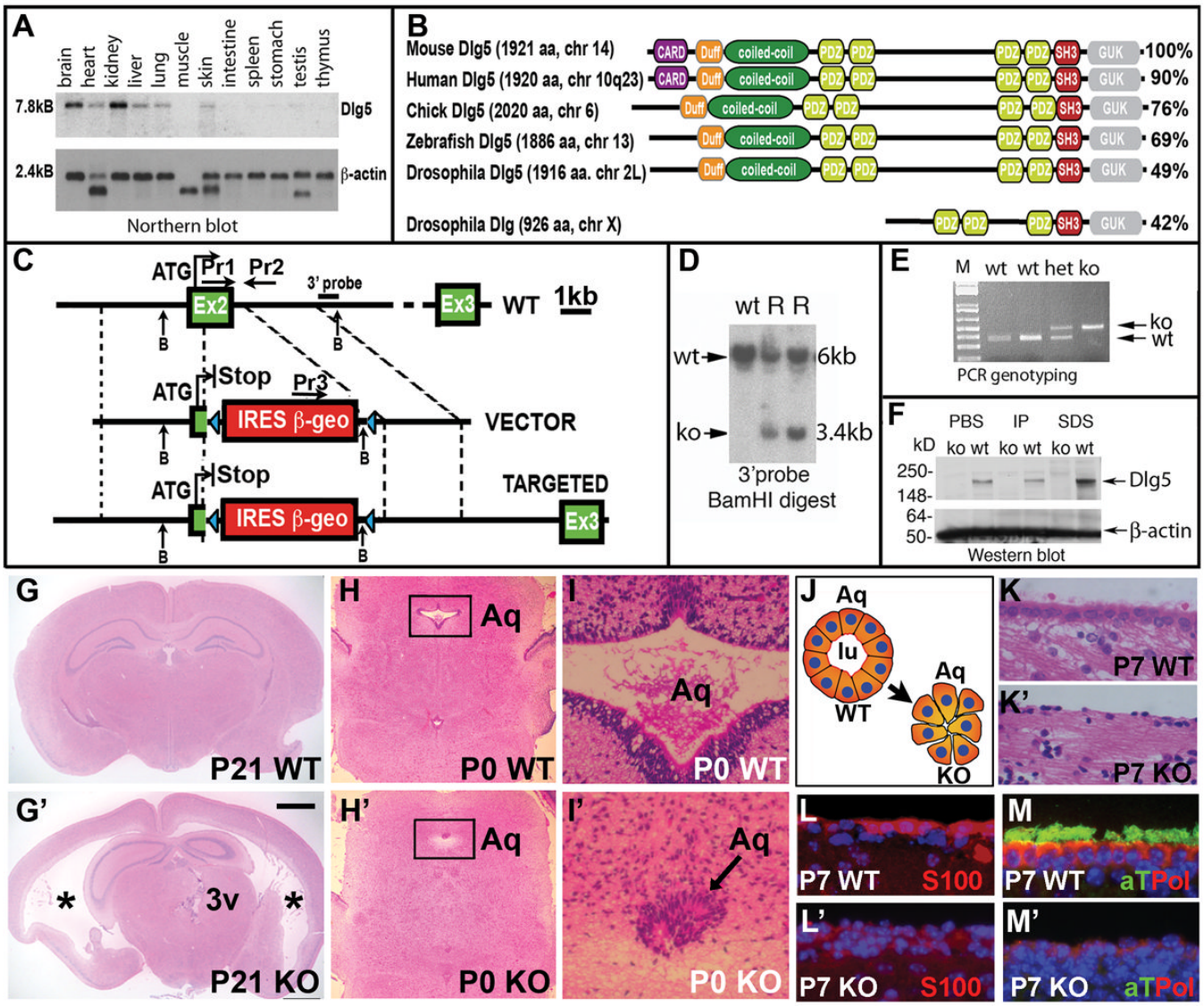

Figure 1. Fusion of the aqueduct, failure of ependymal cell differentiation and severe hydrocephalus in *Dlg5*$^{-/-}$ mice

(A) Expression pattern of *Dlg5* in adult mouse organs. Northern blot analysis with *Dlg5* and *β-actin* probes. **(B)** Domain organization of mouse, human, chick, zebrafish and Drosophila Dlg5 proteins and Drosophila Dlg. Numbers on the right denote percent similarity between mouse Dlg5 and Dlg5 in other species. **(C)** Generation of *Dlg5* knockout mice. Schematic representation of wild-type (WT) allele, targeting vector (VECTOR) and resulting targeted allele (TARGETED). ATG indicates the initiating methionine in exon 2. **(D)** Southern blot analyses of wild-type (WT) and targeted (KO) ES clones with 3′ probe outside the targeting construct. **(E)** PCR amplification of wild-type and knockout alleles from heterozygous (het) and knockout (ko) mice using primers 1, 2 and 3, shown in (C). **(F)** Western blot analyses of proteins extracted from P7 brains of *Dlg5*$^{-/-}$ and wild-type animals using sequential extraction with phosphate-buffered saline (PBS), 1% Triton-X100 buffer (IP) and 1% SDS. Blot was analyzed with anti-Dlg5 and anti-β-actin antibodies. **(G-G')** Haematoxylin & eosin (H&E) stainings of coronal hippocampal sections from P21 wild type (WT) and *Dlg5*$^{-/-}$ (KO) brains. Note severe dilation of the lateral ventricles in *Dlg5*$^{-/-}$ brain (asterisks) and disorganization of

the 3rd ventricle (3V). **(H-I')** H&E stainings of coronal brain sections at the level of aqueduct. Boxed areas containing aqueduct in H-H' are shown at higher magnification in I-I'. Note closure of aqueduct (Aq, arrow) in *Dlg5*$^{-/-}$ mice. **(J)** Model of ventricular tube defect in *Dlg5*$^{-/-}$ brains. Apical surfaces of cells forming the tube are facing the lumen (lu). **(K-M')** Lateral ventricular surfaces from P7 mice stained with H&E (K-K'), anti-S100 (ependymal cell marker) (L-L'), anti-acetylated tubulin (aT, green, cilia marker) and polaris (Pol, red) (M-M') antibodies. DAPI (blue) in L-M' stains cell nuclei. Note absence of ciliated ependymal cells in *Dlg5*$^{-/-}$ brain. Bar in G' represents 1 mm in G-G', 0.4 mm in H-H', 70 μm in K-K' and 40 μm in L-M'.

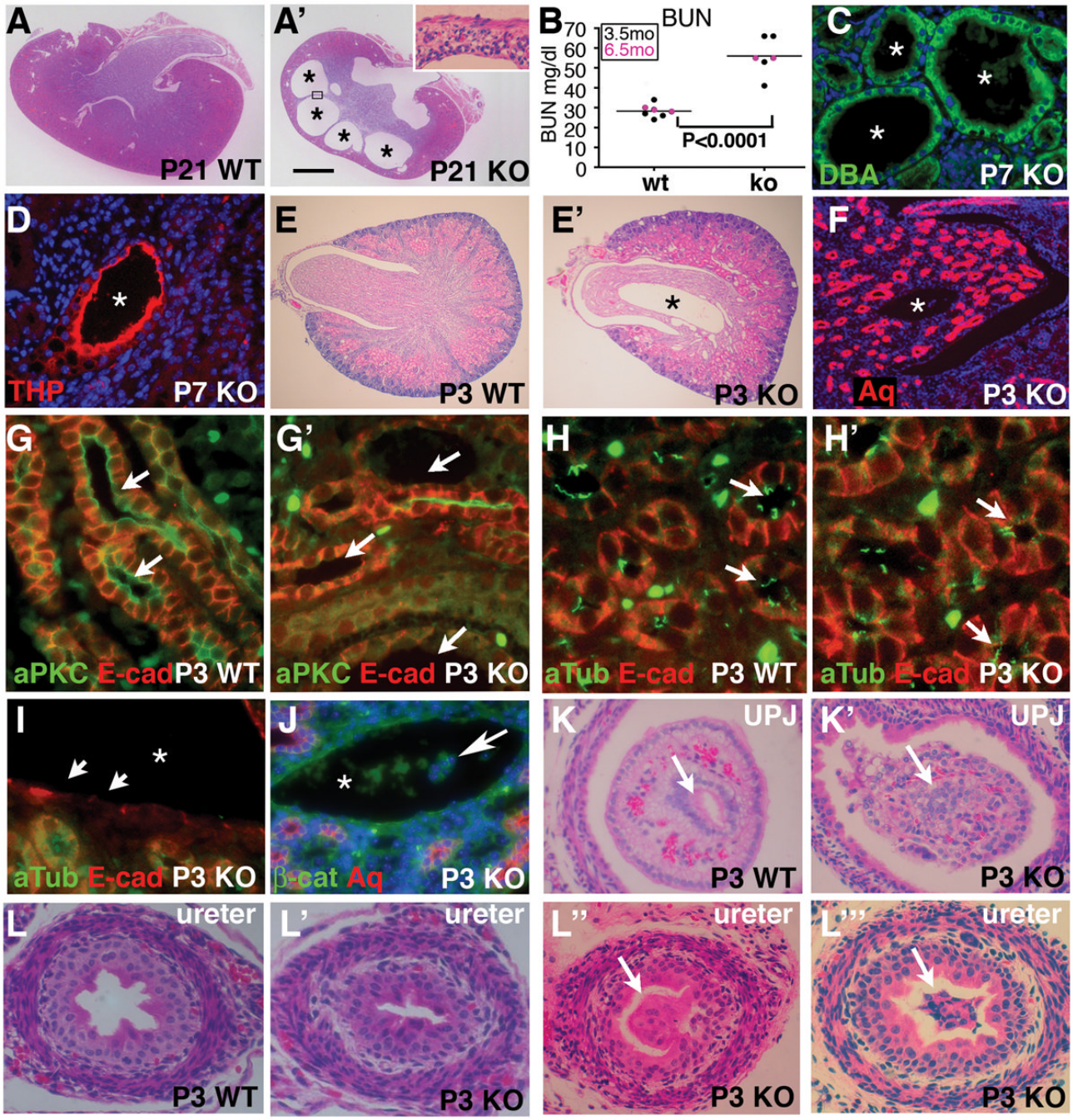

Figure 2. Loss of cell polarity and renal cysts in *Dlg5*$^{-/-}$ mice

(A-A') H&E stainings of kidneys from P21 wild-type (WT) and *Dlg5*$^{-/-}$ (KO) mice. Note multiple cysts (asterisks) in the mutant kidney. Inset in A' shows high magnification of boxed area. **(B)** Blood urea nitrogen (BUN) of 3.5 and 6.5 month-old mutant (ko) and wild-type (wt) mice. P-value was determined by *t*-test. **(C-D)** Immunostaining of P7 early kidney cysts with DBA, marker of collecting ducts, and THP, marker of distal ascending tubules. Only ≤2% of cysts were positive for THP. **(E-E')** H&E stainings of kidneys from P3 wild-type (WT) and *Dlg5*$^{-/-}$ (KO) mice. Note developing cysts in the kidney pelvis (asterisk). **(F)** Immunostaining of *Dlg5*$^{-/-}$ P3 kidney with anti-aquaporin 2 (Aq) antibodies. Note loss of aquaporin-2 in small cyst (asterisk). **(G-G')** Immunostaining of collecting ducts from wild-type (WT) and *Dlg5*$^{-/-}$

(KO) kidneys with anti-aPKC and anti-E-cadherin (E-cad) antibodies. **(H-I)** Immunostaining of collecting ducts from wild-type (WT) and *Dlg5*$^{-/-}$ (KO) kidneys with anti-acetylated tubulin (aTub, cilia marker) and anti-E-cadherin (E-cad) antibodies. Note the loss of tubulin staining in the cyst (asterisk, arrow)(I). **(J)** Immunostaining of kidney from *Dlg5*$^{-/-}$ mice with anti-β-catenin (β-cat) and anti-Aquaporin 2 (Aq) antibodies. Arrow points to loss of cells into the lumen of a small cyst (asterisk). **(K-L‴)** H&E stainings of ureteropelvic junctions (UPJs) and ureters from P3 wild-type (WT) and *Dlg5*$^{-/-}$ (KO) mice. Note disorganization and partial fusion of collecting duct in UPJ (K'), constriction of ureter (L') and ureteral polyps (L"-L‴) in *Dlg5*$^{-/-}$ mice. Bar in A' represents 1 mm in A-A', 0.4 mm in E-E', 150 μm in F, 100 μm in C, D, K-L‴ and 40 μm in G-J.

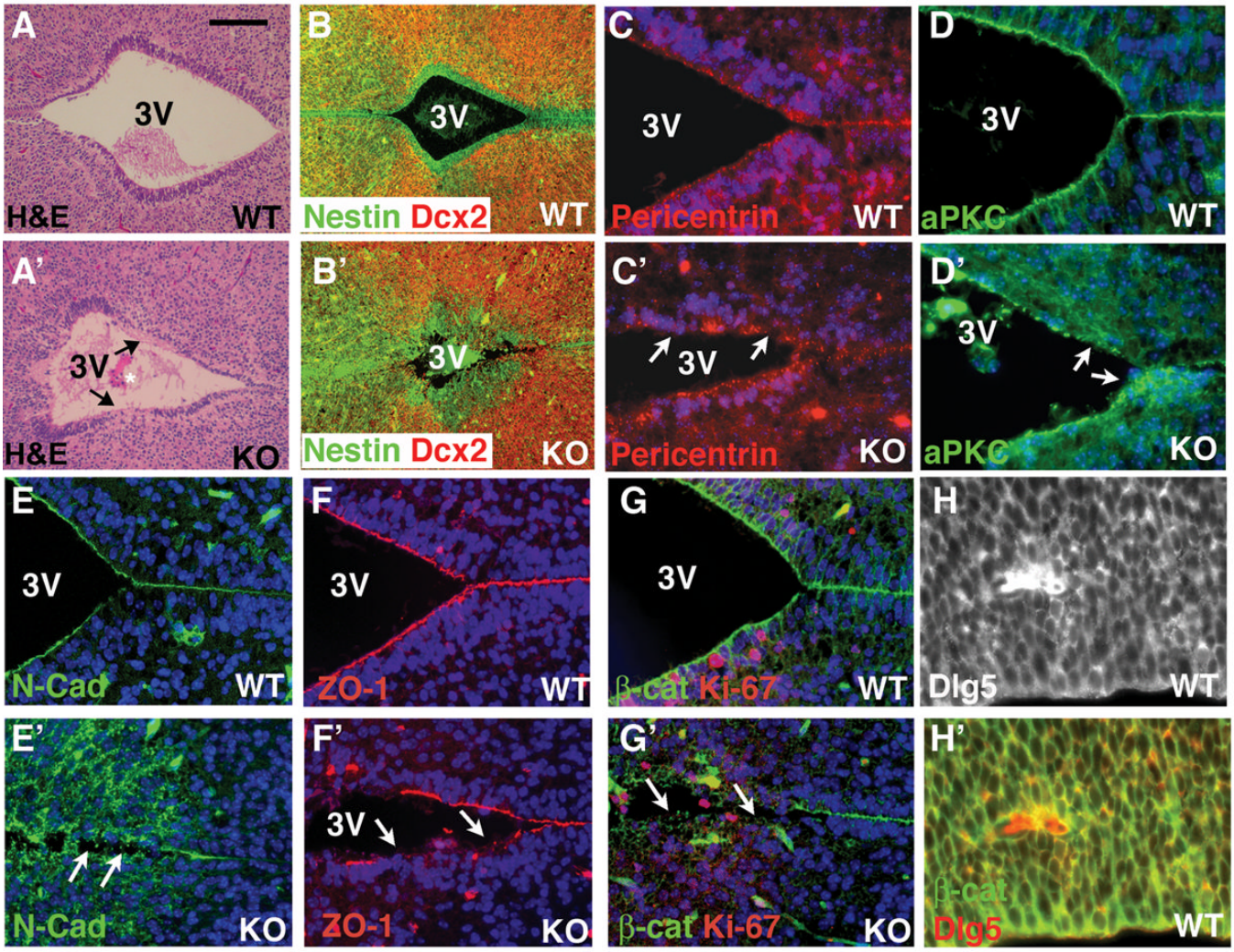

Figure 3. Disruption of adherens junctions and loss of cell polarity as the cellular basis of epithelial tube maintenance defect, closure of the aqueduct and hydrocephalus in *Dlg5*$^{-/-}$ brains

(A-G') Coronal sections from E15.5 *Dlg5*$^{-/-}$ (KO) and wild-type (WT) brains at level of 3rd ventricle stained with H&E (A-A'), anti-Nestin (neural progenitor cell marker) and anti-Dcx2 (newly born neurons) (B-B'), anti-pericentrin (cilia basal body and centrosomal cell polarity marker, B-B'), anti-aPKC (apical membrane cell polarity marker, D-D'), anti-N-cadherin (N-cad, AJ marker, E-E'), anti-ZO-1 (tight and AJ marker) (F-F'), anti-β-catenin (β-cat, AJ marker) and anti-Ki-67 (proliferating cell marker) (G-G'). Note loss of cell polarity and mislocalization of AJ proteins in *Dlg5*$^{-/-}$ progenitors (arrows). **(H-H')** Coronal brain section from E13.5 wild type brain stained with anti-Dlg5 (H) and anti-Dlg5 and anti-β-catenin (H') antibodies. Staining patterns and corresponding antibodies are color-coded. Bar in A represents 100 μm in A-B', 0.3 mm in B-B' 60 μm in C-G' and 40 μm in H-H'.

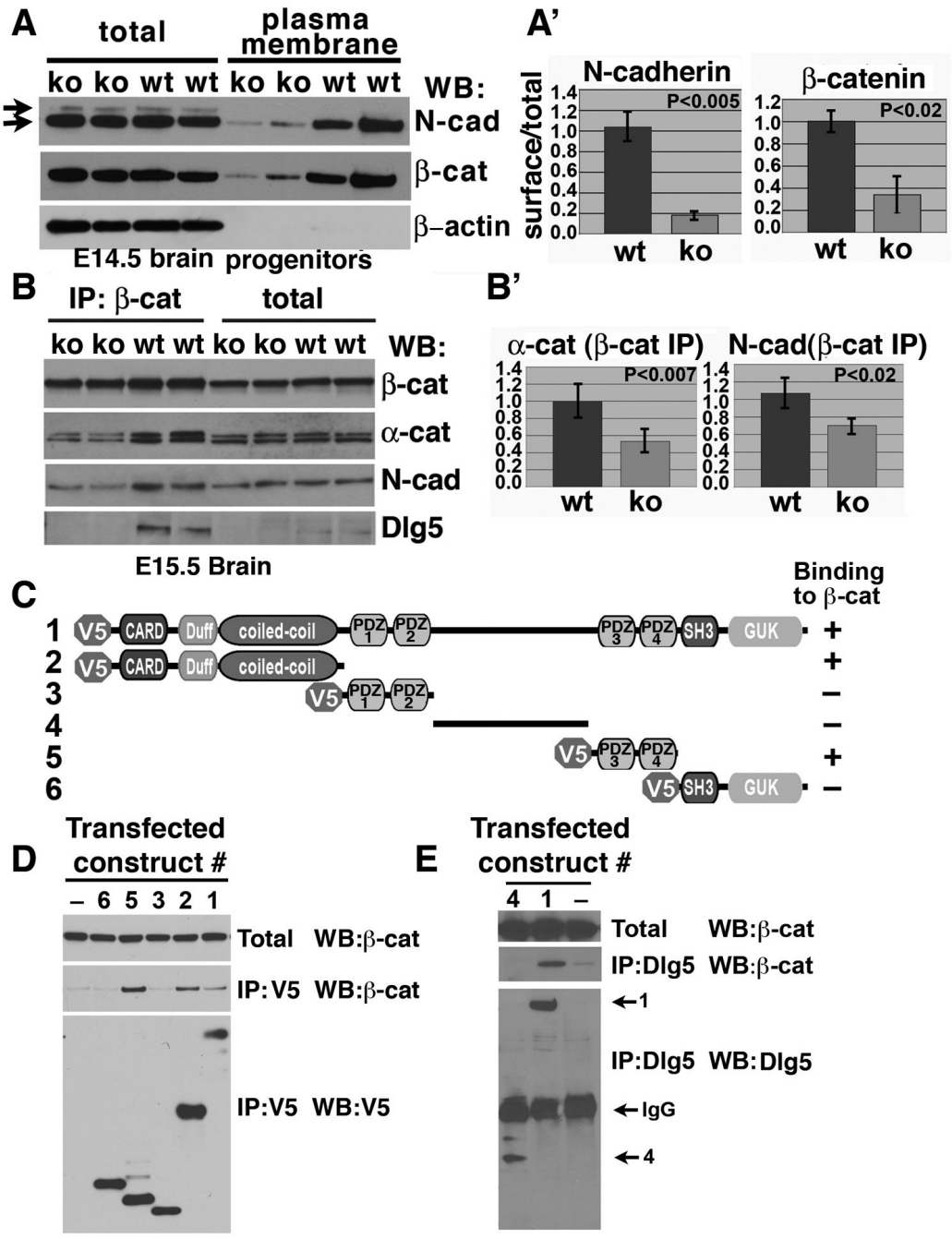

Figure 4. Decrease in cell surface levels and destabilization of AJ protein complexes in *Dlg5*$^{-/-}$ progenitors

(A) Decrease in plasma membrane-associated levels of AJ proteins in *Dlg5*$^{-/-}$ neural progenitors. Cell surface proteins on isolated *Dlg5*$^{-/-}$ (ko) and wild-type (wt) progenitors were biotinylated, immunoprecipitated with streptavidin-sepharose and analyzed by blotting (WB) with anti-N-cadherin (N-cad), anti-β-catenin (β-cat) and anti-β-actin antibodies. Note similar levels of total, but decreased levels of cell surface N-cadherin and N-cadherin-associated β-catenin proteins. Arrows point to the precursor and processed N-cadherin. Note absence of the precursor and β-actin in streptavidin pulldowns. **(A')** Quantitation of experiments similar to the one shown in A. Ratios of plasma membrane to total levels of N-cadherin and β-catenin in

wild-type cells arbitrarily assumed as 1 ± standard error (n=3). P-value was determined by ANOVA test. **(B)** Destabilization of AJ complexes in *Dlg5*$^{-/-}$ brains. Total protein extracts from E15.5 *Dlg5*$^{-/-}$ (ko) and wild-type (wt) brains were immunoprecipitated (IP) with anti-β-catenin (β-cat) antibodies and blotted (WB) with anti-β-catenin, anti-α-catenin (α-cat), anti-N-cadherin (N-cad) and anti-Dlg5 antibodies. (**B'**) Quantitation of experiments similar to the one shown in B. Levels of α-catenin and N-cadherin in β-catenin IPs from wild-type extracts arbitrarily assumed as 1 ± standard deviation (n=4). P-value was determined by ANOVA test. **(C-E)** Identification of Dlg5 domains involved in binding to β-catenin. **(C)** Dlg5 constructs used in immunoprecipitation experiments in (D-E) and summary of binding results. **(D-E)** Indicated Dlg5 constructs were transfected into HEK 293 cells and proteins were immunoprecipitated (IP) with anti-V5 (D) or anti-Dlg5 antibodies directed against part of construct #4(E) and analyzed by blotting (WB) with anti-V5 anti-β-catenin (β-cat) or anti-Dlg5 antibodies.

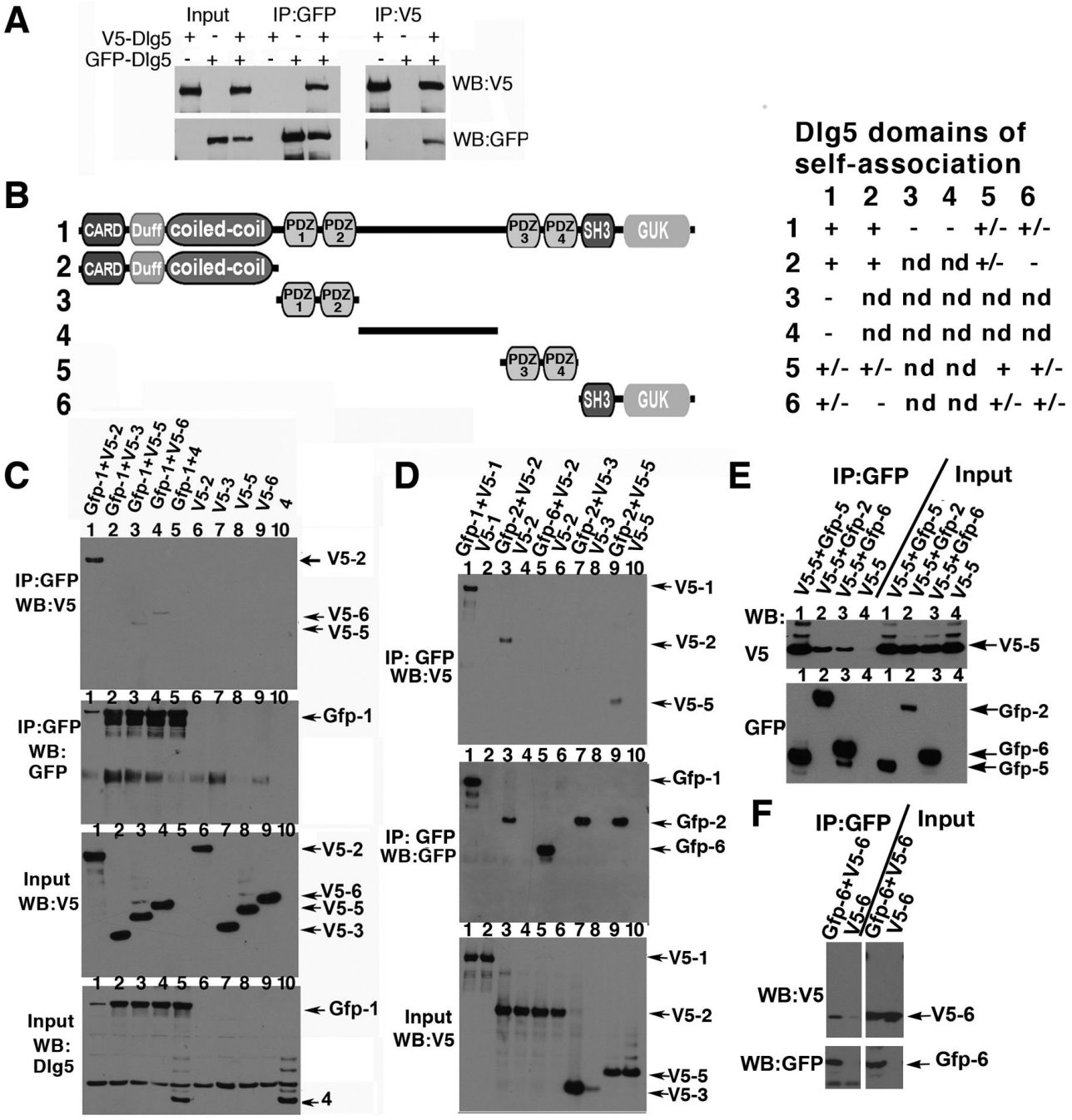

Figure 5. Self-association of Dlg5 and identification of Dlg5 domains responsible for self-association

(A) Self-association of full-length Dlg5. Constructs encoding GFP or V5-tagged Dlg5 proteins were co-transfected into HEK 293 cells. The proteins were immunoprecipitated (IP) with anti-V5 or anti-GFP antibodies and analyzed by Western blotting (WB) with anti-GFP or anti-V5 antibodies. **(B)** Schematic representation of Dlg5 constructs and a summary of binding results. ND indicates "not determined." **(C-F)** Indicated V5-tagged full-length Dlg5 or its fragments or were co-transfected with GFP-tagged full-length Dlg5 or its fragments, immunoprecipitated (IP) with anti-GFP antibodies and analyzed by Western blotting (WB) with anti-V5, anti-GFP and anti-Dlg5 antibodies. Protein tags are as shown. Construct# 4, without tag, was revealed by blotting with anti-Dlg5 antibody. Identity of Dlg5 constructs is encoded by the construct

number shown in B. **(C)** Interaction between full-length Dlg5 and its fragments. Note strong binding of the N-terminal part of Dlg5 containing the coiled-coiled domain (V5-2) and a weaker binding of PDZ-3-4 (V5-5) and SH3-GUK domains of Dlg5 (V5-6). **(D)** Interaction between N-terminal part of Dlg5 (GFP-2 or V5-2) and other Dlg5 fragments that bind to full-length Dlg5. Note self-association of N-terminal part of Dlg5 (V5-2 and GFP-2) and binding to PDZ3-4 (V5-5). **(E)** Interaction between PDZ-3-4 domains of Dlg5 (V5-5, GFP-5) and other Dlg5 fragments that bind to full-length Dlg5. Note self-association of PDZ-3-4 domains of Dlg5 (V5-5 and GFP-5) as well as its binding to N-terminal part of Dlg5 (GFP-2) and C-terminal SH3-GUK domains (GFP-6). **(F)** Self-association of C-terminal SH3-GUK domain of Dlg5 (GFP-6 and V5-6).

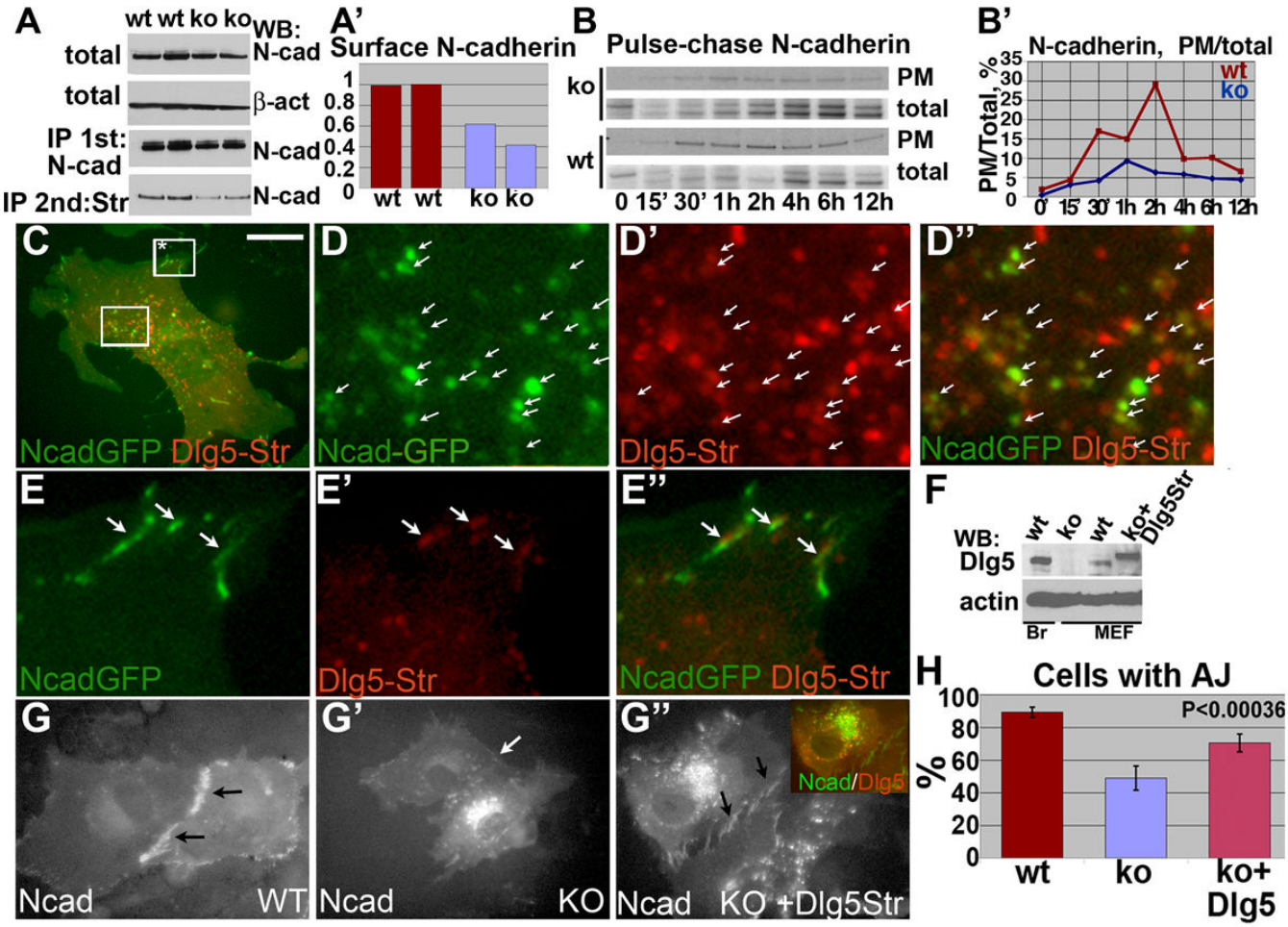

Figure 6. Dlg5 associates with cadherin-carrying transport vesicles and it is necessary for membrane delivery and stabilization of cadherin-catenin complexes

(A) Decreased levels of cell-surface N-cadherin in *Dlg5*$^{-/-}$ MEFs. Total proteins from cell-surface biotinylated MEFs were sequentially immunoprecipitated (IP) with anti-N-cadherin antibodies and streptavidin beads and analyzed by immunoblotting with anti-N-cadherin (N-cad) antibodies. **(A')** Quantitation of the experiment shown in A. Ratios of cell-surface to total N-cadherin in wild-type cells arbitrarily assumed as 1. **(B)** Decrease in cell-surface delivery and stabilization of N-cadherin in *Dlg5*$^{-/-}$ MEFs. Pulse-chase analysis of cell-surface ^{35}S-methionine/cysteine-labeled N-cadherin. **(B')** Quantitation of experiment shown in B. Graph displays ratios of surface to total levels of ^{35}S-labeled N-cadherin in wild-type (WT) and knockout (KO) cells at different time points. **(C-E")** Dlg5 co-localizes with newly-synthesized N-cadherin on the cytoplasmic vesicles and at the AJs in live MEFs. Wild-type MEFs were electropotated with N-cadherin-GFP (Ncad-GFP, green) and Stawberry-Dlg5 (Dlg5-Str, red) constructs. Localization of GFP and Strawberry proteins was detected by live cell microscopy. Areas in boxes in C that contain transport vesicles (lower box) and AJ (upper box) are shown at higher magnification in D-D" and E-E", respectively. White arrows denote co-localization between N-cadherin and Dlg5 proteins. **(F)** Total protein extracts from wild-type (wt) brain (Br), *Dlg5*$^{-/-}$ (ko) and wild-type (wt) MEFs and *Dlg5*$^{-/-}$ MEFs electroporated with Strawberry-Dlg5 expression construct (ko+Dlg5) were analyzed by blotting with anti-Dlg5 and anti-β-actin antibodies. **(G-G")** Wild-type (WT) and *Dlg5*$^{-/-}$ (KO) MEFs were electroporated with N-cadherin-GFP (G-G') or N-cadherin-GFP and Strawberry-Dlg5 (G") constructs and imaged for GFP and Strawberry. Note prominent localization of N-cadherin-GFP to cell-cell junctions

in wild-type (G), but not in *Dlg5*$^{-/-}$ MEFs (G') and rescue of this defect in *Dlg5*$^{-/-}$ MEFs co-transfected with Strawberry-Dlg5 (G"). **(H)** Quantitation of experiments shown in G-G". Percentage of transfected cells (n=60-110) showing junctional staining for N-cadherin-GFP was quantified and statistical significance was determined by ANOVA analysis. Bar in C represents 10 μm in C, 8 μm in G-G", 2 μm in D-E".

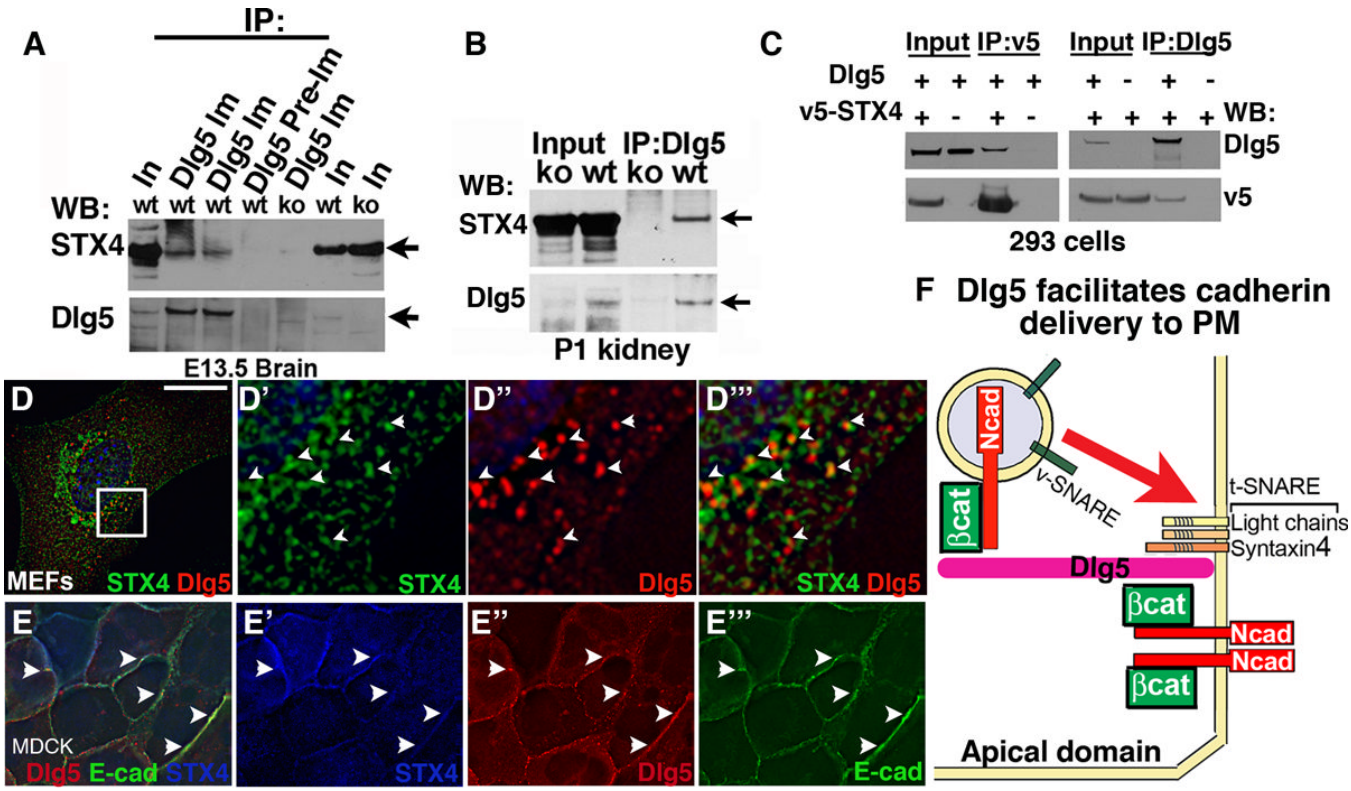

Figure 7. Interaction between Dlg5 and Syntaxin 4, a t-SNARE protein involved in basolateral vesicle transport

(A-B) Association between endogenous Dlg5 and Syntaxin 4 (STX4) proteins in E13.5 brains (A) and P1 kidneys (B). Total protein lysates were immunoprecipitated (IP) with anti-Dlg5 immune and pre-immune serum and analyzed by blotting (WB) with anti-Dlg5 or anti-syntaxin 4 antibodies. **(C)** Co-immunoprecipitation of full-length Dlg5 and Syntaxin 4 proteins expressed in HEK 293 cells. Dlg5 construct was co-transfected with V5-tagged Syntaxin 4 (STX4) and immunoprecipitates with anti-Dlg5 or anti-V5 antibodies were analyzed by Western blotting with anti-Dlg5 or V5 antibodies. **(D)** Co-localization of Dlg5(red) and Syntaxin 4(green) in MEFs, electroporated with the fluorescently-labeled Strawberry-Dlg5 and V5-Syntaxin 4, fixed, and stained with anti-V5 antibody. **E)** Co-localization of Syntaxin 4 (blue) with Dlg5 (red) and E-cadherin (green). V5-Syntaxin4 construct was electroporated into MDCK cells stably expressing Strawberry-Dlg5 and E-cadherin-GFP, cells were fixed and stained with anti-syntaxin 4 antibody. **(F)** Model of Dlg5 function in plasma membrane delivery of cadherin-catenin adhesion complexes by linking t-SNARE vesicle targeting complex with N-cadherin/β-catenin carrying transport vesicles. Bar in D represents 15 μm in D, 2 μm in D'-D‴, 25 μm in E-E‴.